Differentiation of Myeloma and Metastatic Cancer in the Spine Using Dynamic Contrast Enhanced MRI

Ning Lang[a], **Min-Ying Su**[b,*], **Hon J. Yu**[b], **Muqing Lin**[b], **Mark J. Hamamura**[b], and **Huishu Yuan**[a,*]

[a]Department of Radiology, Peking University Third Hospital, Beijing, China

[b]Tu & Yuen Center for Functional Onco-Imaging, Department of Radiological Sciences, University of California, Irvine, CA, USA

Abstract

Spinal myeloma and metastatic cancer cause similar symptoms and show similar imaging presentations, thus making them difficult to differentiate. In this study, dynamic contrast-enhanced MRI (DCE-MRI) was performed to differentiate between nine myelomas and 22 metastatic cancers that present as focal lesions in the spine. The characteristic DCE parameters, including the peak signal enhancement percentage (SE%), the steepest wash-in SE% during the ascending phase, and the wash-out SE% were calculated by normalizing to the pre-contrast signal intensity. The two-compartmental pharmacokinetic model was used to obtain K^{trans} and k_{ep}. All nine 9 myelomas showed the wash-out DCE pattern. Of the 22 metastatic cancers, 12 showed wash-out, seven showed plateau, and three showed persistent enhancing patterns. The fraction of cases that showed the wash-out pattern was significantly higher in the myeloma group than the metastatic cancer group (9/9=100% vs. 12/22=55%, $P = 0.03$). Compared to the metastatic cancer group, the myeloma group had a higher peak SE% (226±72% vs. 165±60%, $P = 0.044$), a higher steepest wash-in SE% (169±51% vs. 111±41%, $P = 0.01$), a higher K^{trans} (0.114±0.036 vs. 0.077±0.028 l/min, $P = 0.016$), and a higher k_{ep} (0.88±0.26 vs. 0.49±0.23 1/min, $P = 0.002$). The receiver operating characteristic (ROC) analysis to differentiate between these two groups showed that the area under the curve was 0.798 for K^{trans}, 0.864 for k_{ep}, and 0.919 for combined K^{trans} and k_{ep}. These results show that DCE-MRI may provide additional information for making differential diagnosis to aid in choosing the optimal subsequent procedures or treatments for spinal lesions.

Keywords

Myeloma; Metastatic cancer; Spine; Dynamic-Contrast-Enhanced MRI; Differential Diagnosis

1. INTRODUCTION

Myeloma and metastatic cancer are commonly seen malignant cancers in the spine. They both affect the bone marrow, present as single or multiple lesions, and show similar

*Corresponding Author (in USA): Min -Ying Su, PhD, 164 Irvine Hall, University of California, Irvine, CA 92697-5020, Tel: (949) 824-4925, Fax: (949) 824-3481, msu@uci.edu. *Corresponding Author (in China): Huishu Yuan, MD, Department of Radiology, Peking University Third Hospital, 49 North Garden Road, Haidian District, Beijing, 100191, PR China, Tel: +86-10-82264747; Fax: +86-10-62017700; huishuy@bjmu.edu.cn.

manifestations in imaging [1]. Magnetic resonance imaging (MRI) is the most useful imaging modality for diagnosing lesions in the spine. It was found that the signal intensity of lesions (pre-or post-Gd), peri-tumor edema, and vessels and nerves surrounding tumors shown on conventional MRI are not specific to differentiate between benign and malignant spinal lesions or among different types of malignant lesions [2–7]. Dynamic contrast enhanced MRI (DCE-MRI) acquires a time series of multiple images after injection of a contrast agent. These images can reveal changes in the contrast features of lesions at different times, providing additional information for diagnosis [8]. In the spine, DCE-MRI has been applied to characterize the normal bone marrow and hematological malignancy of different origins and grades/stages [9–20], but so far there is no report of differentiating between myeloma and metastatic cancer.

Correct diagnosis of spinal lesions based on imaging would help in guiding biopsy and subsequent treatment planning. Especially for patients who do not have a known primary cancer, a correct diagnosis would provide very important information for choosing the most appropriate work-up procedures. DCE-MRI is the standard imaging method for the diagnosis of breast and prostate lesions [21–22]. Inspired by the success of DCE-MRI for the diagnosis of breast and prostate cancer, in this work we evaluate its ability to differentiate between myeloma and metastatic cancer.

Tumors need angiogenesis to sustain rapid growth. In general, there is a higher expression of the vascular endothelial growth factor (VEGF) that stimulates the formation of new vessels. These new vessels are immature and leakier (that is, they have wider endothelial junctions). These features allow contrast agents to quickly leak from the vascular space into the interstitial space and diffuse back into the vascular space for clearance [23]. DCE-MRI can be used to measure the trans port kinetics of contrast agents in the tissue, allowing for the analysis of parameters associated with vascular perfusion, volume, and permeability [24–26]. Several characteristic DCE parameters can be directly measured from the time course, including the peak enhancement, the increase of enhancement during the wash-in phase, and the decrease of enhancement during the wash-out phase. Also, the 2-compartmental pharmacokinetic model can be applied to extract the transfer constant K^{trans} and the rate constant k_{ep} [24–25].

In this study, we measured the enhancement time course of myelomas and metastatic cancers and compared the DCE kinetics between the se two groups. In addition to evaluating the pattern of DCE curves, the heuristic analysis method and pharmacokinetic model fitting were applied to measure the peak enhancement and the steepest wash-in and wash-out enhancements, as well as K^{trans} and k_{ep}. Use of these parameters to differentiate between myeloma and metastatic cancer groups was assessed using the receiver operating characteristic (ROC) analysis to investigate the ability of DCE-MRI to differentiate between these two main malignant entities in the spine.

2. MATERIALS AND METHODS

2.1 Patients

This was a retrospective study. The MRI examinations of patients who had focal lesions in the spine that were confirmed as myeloma or metastatic cancers were identified for analysis. A total of 9 myeloma cases and 22 metastatic cancer cases performed between June 2008 and June 2011 that included a DCE sequence were found. All patients were suspected to have lesions compressing the spinal cord that caused symptoms and were referred to receive an MRI examination for diagnosis. Of the 9 myeloma patients, 8 patients had multiple myeloma and 1 patient had a single lesion. Their mean age was 58 years old. Of the 22 patients with metastatic cancer, 17 patients had multiple lesions and 5 patients had a single

lesion. Their mean age was 55 years old. The primary cancers were lung cancer (7 cases), thyroid cancer (5 cases), liver cancer (4 cases), breast cancer (3 cases), kidney cancer (2 case), and prostate cancer (1 case). This study was approved by the Medicinal Ethics Committee of the Peking University Third Hospital.

2.2 MRI Protocol

MR scans were performed on a 3T Trio scanner (Siemens, Germany). The imaging protocol included transversal T2-weighted imaging (T2WI), sagittal T2WI with and without fat suppression, and sagittal T1-weigthed imaging (T1WI). After the abnormal region was identified using the T1WI and T2WI acquisitions, DCE-MRI was performed using the three -dimensional volume interpolated breath-hold examination (3D VIBE) sequence in the transversal plane to further examine that region. The scan parameters were set to TR = 4.1 ms, TE = 1.5 ms, flip angle = 10°, acquisition matrix = 256×192, and FOV= 250×250 mm. Approximately 30 slices with 3 mm thickness were prescribed to cover the abnormal vertebrae. The temporal resolution varied slightly from 10 to 14 seconds. The difference in imaging time was due to the different number of slices that were needed to cover the abnormal segment of the spine for different patients. The contrast agent, 0.2 mmol/kg Gd-DTPA, was injected after one set of pre-contrast images were acquired using an Ulrich power injector at a rate of 2 ml/sec followed by a 20 cc saline flush at the same rate. A total of 12 frames were acquired, so the total DCE-MRI acquisition time ranged from 120 to 160 seconds.

2.3 Image Analysis to Measure DCE Kinetics

Images were reviewed by two radiologists (NL and HY) with 7 and 19 years of experience in the diagnosis of spine disease using MRI. The area containing the highest enhancement within one imaging slice was selected as the region of interest (ROI) by manual drawing. Because the ROI-based analysis is the most commonly used method in a clinical setting, we chose this method so that the results obtained in this study can be easily applied in future clinical readings. The ROI size ranged from 0.5 to 1 cm^2, with caution taken to exclude cysts, calcification, necrosis, and hemorrhage. The signal intensity time course from the defined ROI was measured using the Siemens Syngo Mean Curve software. The enhancement time course was classified into three types: 1) the wash-out pattern -- the signal intensity increased over 30% during the first 30 s ascending phase, reached a peak, then decreased (wash-out) with a greater than 10% drop from the peak; 2) the plateau pattern -- the signal intensity increased over 30% during the first 30 s ascending phase, then reached a plateau phase; and 3) the persistent enhancement pattern -- the signal intensity increased over 10% but less than 30% during the first 30 s ascending phase, then continued to enhance during the remaining DCE period. When the signal intensity increased no more than 10% during the first 30s ascending phase, the lesion was not well enhanced and the DCE pattern cannot be characterized.

2.4 Analysis of Characteristic DCE Parameters

Based on the averaged signal intensity over the selected ROI, each case has only one signal intensity time course for analysis. Several characteristic parameters can be extracted based on this enhancement time course. The MR images were acquired using a spine surface coil, where the signal intensity may vary substantially depending on the location of the abnormal segment. Therefore, the measured signal enhancement needs to be normalized to the pre-contrast signal intensity to convert to percent enhancement. The maximum signal intensity (SI) across all measured time points was used to calculate the peak enhancement using Eq. (1),

$$\text{Peak SE\%} = \frac{\text{SI}_{\text{peak}} - \text{SI}_{\text{initial}}}{\text{SI}_{\text{initial}}} \times 100\%. \quad (1)$$

SI_{peak} is the peak signal intensity across all time points and $\text{SI}_{\text{initial}}$ is the pre-contrast signal intensity before contrast agent injection. Next, the steepest wash-in segment during the ascending phase was determined by identifying the two adjacent time points (SI_2 and SI_1) that show the largest increase in signal intensity. This change in signal intensity along with the baseline SI was used to calculate the steepest wash-in SE% using Eq. (2),

$$\text{Steepest Wash-in SE\%} = \frac{\text{SI}_2 - \text{SI}_1}{\text{SI}_{\text{initial}}} \times 100\%. \quad (2)$$

For those curves that show the wash-out pattern, the wash-out % was calculated as the decrease in signal intensity between the peak and the end time points divided by the pre-contrast SI, as shown in Eq. (3),

$$\text{Wash-out SE\%} = \frac{\text{SI}_{\text{peak}} - \text{SI}_{\text{end}}}{\text{SI}_{\text{initial}}} \times 100\%. \quad (3)$$

For those curves that did not show the wash-out pattern, this wash-out SE% could not be calculated.

2.5 Analysis of Quantitative Parameters Using Pharmacokinetic Modeling

We also applied two-compartment pharmacokinetic modeling to analyze the quantitative parameters, including the transfer constant K^{trans} (related to wash-in) and the rate contrast k_{ep} (related to wash-out) using the unified Tofts model [24, 25]. The two compartments are the vascular space and the interstitial space. The in-flux transfer constant K^{trans} measures leakage of the contrast agent from the vascular into the interstitial space and the out-flux rate constant k_{ep} measures diffusion of the contrast agent from the interstitial space back into the vascular space. Using this model, the change of concentration in the extravascular-extracellular space (Ce) is expressed in Eq. (4),

$$\frac{d\,\text{Ce}}{\text{dt}} = K^{\text{trans}} \cdot [\text{Cb}] - k_{\text{cp}} \cdot [\text{Ce}]. \quad (4)$$

Another parameter in the model is the distribution volume ve in the extravascular-extracellular space (within the interstitial space), which can be calculated as $K^{\text{trans}}/k_{\text{ep}}$. The vascular kinetics Cb is required for the pharmacokinetic fitting and is modeled as a bi-exponential decay function as expressed in Eq. (5),

$$\text{Cb}(t) = D[a1 \exp(-m1\,t) + a2 \exp(-m2\,t)]. \quad (5)$$

The fast decay component is related to the quick distribution of the injected contrast agents to the whole body and the slow delay component is related to the diffusion of contrast agents from whole body back to the blood to be cleared by the kidneys. For data fitting to obtain K^{trans} and k_{ep}, we used the same blood kinetic parameters used in the commercial software syngo Tissue 4D (Siemens), which is based on the blood curves reported by Parker et al. [27]. These parameters are: D = 0.2 mmol/kg, a1= 92.0 kg/L, a2 = 6.4 kg/L, m1= 5.3 1/min, and m2= 0.016 1/min. Since it is impractical to measure the T1 value of each individual

lesion in a clinical protocol, the pre-contrast T1 relaxation time to be used in the pharmacokinetic analysis is assumed to be 1.5 seconds for all lesions. Since myeloma and metastatic cancers could not be differentiated on pre-contrast T1-weighted images, it is reasonable to assume an identical T1 value for all lesions. In order to take into account the slightly different contrast agent injection times, an offset to adjust the time t = 0 in the DCE time course was included in the fitting. The fitting quality was visually inspected and the R^2 value was calculated for quantitative evaluation.

2.6 Statistical Analysis

The DCE pattern for each case was categorized as wash-out, plateau, or persistent enhancement. The fraction of different patterns in the myeloma and metastatic cancer groups were compared using the Fisher's Exact test. The characteristic DCE parameters (peak SE%, steepest wash-in SE%, wash-out SE%) and the pharmacokinetic parameters (K^{trans} and k_{ep}) between the myeloma and metastatic cancer groups were compared using the 2-tailed Student's T-test. All analysis was performed using the SPSS 11.5 software, with $P < 0.05$ being regarded as significant. In addition, the ROC analysis was performed to evaluate the diagnostic ability of each analyzed parameter along with combined parameters (based on logistic regression) to differentiate between the myeloma and metastatic cancer groups using version 11.4 of MedCalc (Mariakerke, Belgium).

3. RESULTS

3.1 DCE Kinetic Patterns

All 9 myeloma (9/9 = 100%) showed the wash-out pattern in their DCE kinetics. Of the 22 metastatic cancer cases, 12 cases (12/22 = 54%) showed the wash-out pattern, 7 cases (7/22 = 32%) showed the plateau pattern, and 3 cases (3/22 = 14%) showed the persistent enhancing pattern. The difference in the fraction showing the wash-out pattern between the two types of cancers was significant, with $P = 0.03$. For the 9 myeloma and the 12 metastatic cancers that show wash-out, the mean ± standard deviation wash-out SE% (between the maximum and the last time points) was 59±29% for the 9 myelomas and 36±19% for the 12 metastatic cancers. Figure 1 and Figure 2 show two examples of myeloma cases. Figure 3 shows a metastatic thyroid cancer with the wash-out DCE pattern and Figure 4 shows a metastatic breast cancer with the plateau DCE pattern.

3.2 DCE Characteristic/Pharmacokinetic Parameters

The characteristic DCE parameters and the pharmacokinetic parameters in the myeloma and the metastatic cancer groups are summarized in Table 1. Compared to the metastatic cancer group, the myeloma group has a higher peak signal enhancement (peak SE% = 226±72% vs. 165± 60%, $P = 0.044$) and a faster wash-in SE% between two adjacent time points during the ascending phase (steepest wash-in SE% = 169± 51% vs. 111±41%, $P = 0.01$). The K^{trans} and k_{ep} obtained from the pharmacokinetic modeling analysis showed consistent results. The transfer constant K^{trans} was significantly higher in the myeloma group compared to the metastatic cancer group (0.114±0.036 vs. 0.077±0.028 l/min, $P = 0.016$). The parameter K^{trans} is related to the wash-in phase and its higher value in the myeloma group is consistent with a higher peak SE% and a higher wash-in SE%. The rate constant k_{ep} was also significantly higher in the myeloma group compared to the metastatic cancer group (0.88±0.26 vs. 0.49±0.23 l/min, $P = 0.002$). The parameter k_{ep} is related to the wash-out phase and its higher value in the myeloma group is consistent with more cases showing the wash-out pattern and the higher wash-out SE%.

3.3 ROC Analysis

The ROC analysis was performed to differentiate between the myeloma and metastatic cancer groups. The area under the curve (AUC) was calculated as 0.737 for peak SE%, 0.803 for the steepest wash-in SE%, 0.798 for K^{trans}, and 0.864 for k_{ep}. Since only 12 cases out of the 22 metastatic cancers had the wash-out SE%, the ROC analysis was not performed for this parameter. It can be seen that among all analyzed parameters, k_{ep} has the highest AUC and the peak SE% has the lowest AUC. When K^{trans} and k_{ep} were combined, the AUC further increased to 0.919, as shown in Figure 5. However, when all 4 parameters were combined, the AUC was only 0.909.

3.4 DCE Parameters in Metastatic Tumors of Different Primary

The metastatic cancer group is heterogeneous, comprised of several different primary cancer types, including 7 lung, 5 thyroid, 4 liver, 3 breast, 2 kidney, and 1 prostate. The characteristic DCE parameters and the fitted pharmacokinetic parameters in the different primary cancer subgroups are summarized in Table 2. The number of cases showing wash-out, plateau and the persistent enhancing pattern are indicated. There are no significant differences among these subgroups.

4. DISCUSSION

Spinal myeloma and metastatic tumors both affect bone marrow and have similar morphological imaging presentations in conventional pre- and post-Gd MRI, thus making them difficult to differentiate [1]. In general, it is difficult to differentiate between benign and malignant musculoskeletal lesions in the spine and even more difficult to predict the type of malignant tumors [2–8]. All patients analyzed in this study presented similar symptoms of pain, which were suspected to come from compression of the spinal cord due to the presence of lesions. As shown in the illustrated cases, the imaging features of pre-contrast T1WI and T2WI and post -contrast T1WI are similar. Steolytic destruction and soft tissue mass showing heterogeneous enhancements are the most common imaging features, which cannot be used to differentiate between myeloma and metastatic cancer. As the treatment options and the overall management for these two diseases are different, a correct diagnosis based on imaging will be very helpful for choosing the most suitable subsequent procedures. For myeloma, radiation therapy and chemotherapy are the main treatment options; for metastatic cancer, the patient may need additional work-up to identify the primary cancer and the extent of metastasis for choosing the optimal treatment strategy (which may include surgery, radiation, and chemotherapy).

Tumors require angiogenesis to grow and invade. Angiogenic vessels are distributed abnormally, having uneven diameters and wider endothelial junctions (leakier vessels). The enhancement time course measured by DCE-MRI can be used to evaluate these vascular properties for the diagnosis of diseased vertebrae [28]. In this study, multi-slice and multiphase DCE-MRI was acquired using the FLASH 3D VIBE sequence, which can cover an abnormal region with an in-plane spatial resolution of 1.3×1.0 mm, slice thickness of 3 mm, and temporal resolution of 10–14 seconds. Despite the very short imaging time, the spatial resolution and image quality of the VIBE sequence are sufficient for the evaluation of anatomic features and selection of strongly enhanced tissues for further analysis.

The vascular endothelial growth factor (VEGF) is the most studied angiogenesis stimulating factor and has been shown to be an important factor in the progression of hematological tumor infiltration into normal bone marrow [29–30]. Microvessel density is a common index used to assess the degree of angiogenesis. In myeloma patients, a higher microvessel density has been shown to correlate with higher tumor grade, worse prognosis, and shorter survival [31–32]. Contrast-enhanced MRI can be used to evaluate the infiltration pattern and provide

very important diagnostic/prognostic information [9] and has been recommended as a supplement for the clinical staging of multiple myeloma [33]. Several DCE-MRI studies using the heuristic or a simple pharmacokinetic model have also shown that the imaging results are correlated to clinical and pathological findings and the patient's survival [15–18]. Therefore, MRI can provide very useful information for myeloma patients.

DCE-MRI is the standard protocol used for the diagnosis of breast and prostate cancer by MRI [21–22]. It has been widely used for evaluating many other types of cancers, but there has been no report yet for differentiating between myeloma and metastatic spinal lesions. In this study, we found that myeloma and metastatic cancers have significantly different DCE kinetics, either using the evaluation of curve patterns, heuristic analysis of DCE characteristic parameters, or a more sophisticated pharmacokinetic modeling analysis. Overall, the myeloma group showed a more aggressive type of DCE kinetics compared to the metastatic cancer group. All 9 myeloma cases showed the wash-out DCE pattern, which is associated with a high vascular volume and a high vascular permeability. This pattern may also be associated with a high cellular density, which limits the distribution of contrast agents into the extravascular-extracellular space. From histological examination, spinal myeloma shows high cellular density with little interstitial space. Therefore, contrast agents can quickly fill up this limited space then rapidly diffuse back to the bloodstream for clearance.

In contrast, the DCE pattern for the metastatic cancer group is more diverse. Of the 22 tumors, 12 showed the wash-out pattern, 7 showed the plateau pattern, and 3 showed the persistent enhancing pattern. The histopathological presentation of metastatic cancer can vary substantially and show diverse vascular and cellular characteristics. Compared to the wash-out DCE pattern, the plateau or the persistent enhancement DCE pattern may indicate a lower vascular volume (supplying less contrast agents), a lower vascular permeability, and/or a higher interstitial space for contrast agents to diffuse far away from the vessel (that is, a lower cellular density). We also analyzed the metastatic cancers originating from different types of primary cancer, as shown in Table 2, but did not find significant differences among the different subtypes.

Heuristic analysis of the DCE time course is commonly used to obtain semi-quantitative characteristic parameters for further comparison. We analyzed the peak enhancement and the steepest wash-in and wash-out percent enhancements. Compared to the metastatic cancer group, the myeloma group has a higher maximum enhancement (peak SE%) and a faster wash-in SE%, indicating a larger quantity and faster uptake of the contrast agent supplied by a higher vascular volume or perfusion.

Pharmacokinetic model fitting was used to obtain the parameters K^{trans} and k_{ep}. We used the blood kinetics used in the commercial software Tissue 4D, which was based on the blood curve published by Parker et al [27]. By choosing the same blood parameters as those used in this commercial software, our results can be easily compared to others analyzed using this program. Consistent with the percent enhancement, the myeloma group has a significantly higher K^{trans} and k_{ep} compared to the metastatic cancer group. In the ROC analysis, k_{ep} has the highest AUC of 0.864. The AUC of K^{trans} and the steepest wash-in SE% were close at around 0.8, while the AUC of the peak SE% was lower at 0.737. The DCE curve is dependent on the blood flow, the permeability and surface area of the vessels, and the distribution volume of the extravascular-extracellular space [24–25]. Depending on the transport regime of the contrast agent (which can be flow-limited, permeability-limited, or mixed), different factors may explain the higher K^{trans} and k_{ep} observed in the myeloma group [26].

One limitation of this study is the assumption of an identical pre-contrast T1 value for all lesions. These lesions have a similar appearance on pre and post-contrast T1 weighted images and are thus likely have similar T1 values. However, tumors are very heterogeneous, and without actually measuring the T1 values we cannot assess its actual impact on the derived pharmacokinetic parameters K^{trans} and k_{ep}. Nonetheless, we analyzed the DCE characteristic parameters directly from the signal intensity time course without using the T1 values and obtained results that were similar to the pharmacokinetic analysis results. These consistent findings suggest that assuming an identical T1 value for all lesions is reasonable. In the ROC analysis of the DCE characteristic parameters, we did not include the wash-out SE% due to a high portion of inapplicable data from the metastatic group. Of the 22 lesions, 7 had plateau and 3 had persistent DCE kinetic patterns, both with no wash-out SE%. By selecting two fixed time frames (e.g. the third and the last time points after contrast injection), the enhancement difference can be calculated and used as a parameter. This is a method used in commercial computer-aided diagnosis software for DCE, where the wash-out pattern will show a positive slope, the plateau pattern will have close to a zero slope, and the persistent enhancing pattern will show a negative wash-out slope. However, since the peak enhancement is not considered, the slopes calculated using a fixed frame may not represent the true wash-out. By using the pharmacokinetic analysis, k_{ep} can be derived in all cases. As shown in this work, this parameter has the highest predictive value in the ROC analysis. Lastly, we applied a manual ROI-based method, which only analyzes one enhancement time course based on the mean signal intensity within the selected ROI. By using a pixel-by-pixel analysis, the heterogeneity within a lesion can be further analyzed to obtain additional information. However, this requires more sophisticated image processing procedures. In summary, we have shown that DCE-MRI can provide additional information that cannot be obtained using the conventional MRI protocol to differentiate between myelomas and metastatic cancers. More cases in a larger study need to be analyzed to evaluate the diagnostic value of DCE-MRI for spinal lesions, as well as to build the diagnostic classifier and determine the optimal cut-off values of the quantitative parameters to achieve optimized sensitivity and specificity.

References

1. Kim HJ, Ryu KN, Choi WS, et al. Spinal involvement of hematopoietic malignancies and metastasis: differentiation using MR imaging. Clin Imaging. 1999; 23:125–133. [PubMed: 10416091]

2. Gernaerdt MJA, Hogendoorn PCW, Bolem JL, et al. Cartilaginous tumors: fast contrast-enhanced MR imaging. Radiology. 2000; 214:539–546. [PubMed: 10671608]

3. Moulton JS, Blebea JS, Dunco DM, et al. MR imaging of soft -tissue masses: diagnositic efficacy and value of distinguishing between benign and malignant lesions. Am J Roentgenol. 1995; 164:1191–1199. [PubMed: 7717231]

4. Hermann G, Abdelwahab LF, Miller TT, et al. Tumour and tumour-like conditions of the soft tissue: magnetic resonance imaging features differentiating benign from malignant masses. Br J Radiol. 1992; 65:14–20. [PubMed: 1336692]

5. May DA, Good RB, Smith DK, et al. MR imaging of musculoskeletal tumors and tumor mimickers with intravenous gadolinium: experiences with 242 patients. Skeletal Radiol. 1997; 26:2–15. [PubMed: 9040136]

6. Elemann R, Reiser MF, Peters PE, et al. Musculoskeletal neoplasms: static and dynamic Gd-DTPA enhanced MR imaging. Radiology. 1989; 171:767–773. [PubMed: 2717749]

7. Lang P, Honda G, Roberts T, et al. Musculoskeletal neoplasm: perioneoplastic edema versus tumor on dynamic postcontrast MR imaging with spatial mapping of instantaneous enhancement rates. Radiology. 1995; 197:831–839. [PubMed: 7480764]

8. Verstraete KL, De Deene Y, Roels H, et al. Benign and malignant musculoskeletal lesions: dynamic contrast-enhanced MR imaging-parametric "first-pass" images depict tissue vascularization and perfusion. Radiology. 1994; 192:835–843. [PubMed: 8058957]

9. Stäbler A, Baur A, Bartl R, et al. Contrast enhancement and quantitative signal analysis in MR imaging of multiple myeloma: assessment of focal and diffuse growth patterns in marrow correlated with biopsies and survival rates. AJR Am J Roentgenol. 1996; 167:1029–1036. [PubMed: 8819407]

10. Baur A, Stäbler A, Bartl R, et al. MRI gadolinium enhancement of bone marrow: age -related changes in normals and in diffuse neoplastic infiltration. Skeletal Radiol. 1997; 26:414–418. [PubMed: 9259099]

11. Moehler TM, Hawighorst H, Neben K, et al. Bone marrow microcirculation analysis in multiple myeloma by contrast-enhanced dynamic magnetic resonance imaging. Int J Cancer. 2001; 93:862–868. [PubMed: 11519049]

12. Moulopoulos LA, Maris TG, Papanikolaou N, et al. Detection of malignant bone marrow involvement with dynamic contrast-enhanced magnetic resonance imaging. Ann Oncol. 2003; 14:152–158. [PubMed: 12488307]

13. Montazel JL, Divine M, Lepage E, et al. Normal spinal bone marrow in adults: dynamic gadolinium-enhanced MR imaging. Radiology. 2003; 229:703–709. [PubMed: 14593190]

14. Rahmouni A, Montazel JL, Divine M, et al. Bone marrow with diffuse tumor infiltration in patients with lymphoproliferative diseases: dynamic gadolinium-enhanced MR imaging. Radiology. 2003; 229:710–717. [PubMed: 14593191]

15. Baur A, Bartl R, Pellengahr C, et al. Neovascularization of bone marrow in patients with diffuse multiple myeloma: a correlative study of magnetic resonance imaging and histopathologic findings. Cancer. 2004; 101:2599–2604. [PubMed: 15503306]

16. Nosàs-Garcia S, Moehler T, Wasser K, et al. Dynamic contrast-enhanced MRI for assessing the disease activity of multiple myeloma: a comparative study with histology and clinical markers. J Magn Reson Imaging. 2005; 22:154–162. [PubMed: 15971177]

17. Baur-Melnyk A, Buhmann S, Dürr HR, et al. Role of MRI for the diagnosis and prognosis of multiple myeloma. Eur J Radiol. 2005; 55:56–63. [PubMed: 15950101]

18. Hillengass J, Wasser K, Delorme S, et al. Lumbar bone marrow microcirculation measurements from dynamic contrast-enhanced magnetic resonance imaging is a predictor of event-free survival in progressive multiple myeloma. Clin Cancer Res. 2007; 13:475–481. [PubMed: 17255268]

19. Zhang L, Mandel C, Yang ZY, et al. Tumor infiltration of bone marrow in patients with hematological malignancies: dynamic contrast-enhanced magnetic resonance imaging. Chin Med J (Engl). 2006; 119:1256–1262. [PubMed: 16919184]

20. Hillengass J, Zechmann C, Bäuerle T, et al. Dynamic contrast-enhanced magnetic resonance imaging identifies a subgroup of patients with asymptomatic monoclonal plasma cell disease and pathologic microcirculation. Clin Cancer Res. 2009; 15:3118–3125. [PubMed: 19366830]

21. Turnbull LW. Dynamic contrast-enhanced MRI in the diagnosis and management of breast cancer. NMR Biomed. 2009; 22:28–39. [PubMed: 18654999]

22. Franiel T, Hamm B, Hricak H. Dynamic contrast-enhanced magnetic resonance imaging and pharmacokinetic models in prostate cancer. Eur Radiol. 2011; 21:616–626. [PubMed: 21184082]

23. Barrett T, Brechbiel M, Bernardo M, Choyke PL. MRI of tumor angiogenesis. J Magn Reson Imaging. 2007; 26:235–249. [PubMed: 17623889]

24. Tofts PS, Kermode AG. Measurement of the blood–brain barrier permeability and leakage space using dynamic MR imaging. 1. Fundamental concepts. Magn Reson Med. 1991; 17:357–367. [PubMed: 2062210]

25. Tofts PS. Modeling tracer kinetics in dynamic Gd-DTPA MR imaging. J Magn Reson Imaging. 1997; 7:91–101. [PubMed: 9039598]

26. Tofts PS, Brix G, Buckley DL, et al. Estimating kinetic parameters from dynamic contrast-enhanced T(1)-weighted MRI of a diffusable tracer: standardized quantities and symbols. J Magn Reson Imaging. 1999; 10:223–232. [PubMed: 10508281]

27. Parker GJ, Roberts C, Macdonald A, et al. Experimentally-derived functional form for a population-averaged high-temporal-resolution arterial input function for dynamic contrast-enhanced MRI. Magn Reson Med. 2006; 56:993–1000. [PubMed: 17036301]

28. Tokuda O, Hayashi N, Taguchi K, et al. Dynamic contrast-enhanced perfusion MR imaging of diseased vertebrae: analysis of three parameters and the distribution of the time-intensity curve patterns. Skeletal Radiol. 2005; 34:632–638. [PubMed: 16091963]

29. Moehler TM, Neben K, Ho AD, et al. Angiogenesis in hematologic malignancies. Ann Hematol. 2001; 80:695–705. [PubMed: 11797109]

30. Kimlinger T, Kline M, Kumar S, et al. Differential expression of vascular endothelial growth factors and their receptors in multiple myeloma. Haematologica. 2006; 91:1033–1040. [PubMed: 16870555]

31. Rajkumar SV, Leong T, Roche PC, et al. Prognostic value of bone marrow angiogenesis in multiple myeloma. Clin Cancer Res. 2000; 6:3111–3116. [PubMed: 10955791]

32. Munshi NC, Wilson C. Increased bone marrow microvessel density in newly diagnosed multiple myeloma carries a poor prognosis. Semin Oncol. 2001; 28:565–569. [PubMed: 11740810]

33. Baur A, Stäbler A, Nagel D, et al. Magnetic resonance imaging as a supplement for the clinical staging system of Durie and Salmon? Cancer. 2002; 95:1334–1345. [PubMed: 12216103]
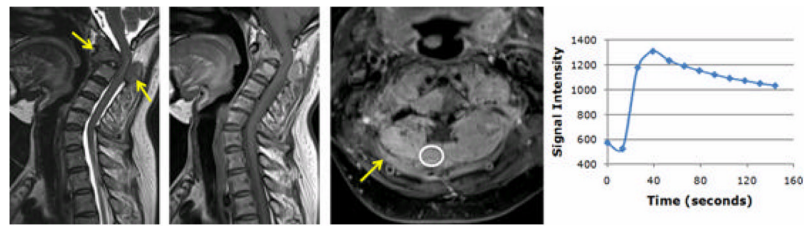
Figure 1.
A 56-year-old female patient with confirmed pathological diagnosis of myeloma. A. MR T2WI and B. MR T1WI show steolytic destruction in the C1-3 vertebral body. A soft tissue mass around the vertebral canal compressing the vertebral body is shown. C. Contrast-enhanced MR T1WI shows a heterogeneously enhanced lesion. D. The DCE kinetics show rapid wash-in with a peak at 40 seconds, followed by wash-out. The peak SE% = 138%, steepest wash-in SE% = 114%, and wash-out SE% = 48%. From pharmacokinetic analysis, the fitted $K^{trans} = 0.069$/min and $k_{ep} = 0.96$/min.
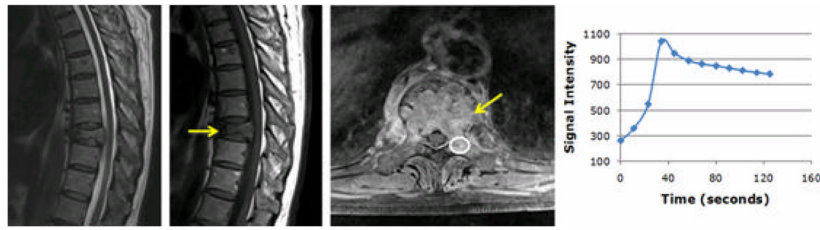
Figure 2.
A 60-year-old male patient with confirmed pathological diagnosis of myeloma. A. MR T2WI and B. MR T1WI show a compressed T9 vertebral body with steolytic destruction. A soft tissue mass leading to narrowing of the vertebral canal is seen. C. Contrast-enhanced MR T1WI shows a heterogeneously enhanced lesion. D. The DCE kinetics show rapid wash-in with a peak at 35 seconds, followed by wash-out. The peak SE% = 300%, steepest wash-in SE% = 188%, and wash-out SE% = 62%. From pharmacokinetic analysis, the fitted K^{trans} = 0.14/min and k_{ep} = 0.98/min.
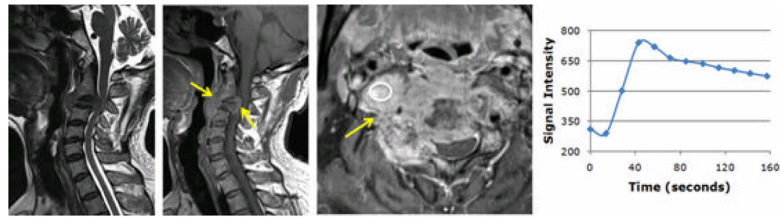
Figure 3.
A 55-year-old male patient with confirmed pathological diagnosis of metastatic cancer originating from the thyroid. A. MR T2WI and B. MR T1WI show steolytic destruction in the C1-3 vertebral body. A soft tissue mass compressing the vertebral body is shown. C. Contrast-enhanced MR T1WI shows a heterogeneously enhanced lesion. D. The DCE kinetics show rapid wash-in with a peak at 45 seconds, followed by wash-out. The peak SE % = 139%, steepest wash-in SE% = 77%, and wash-out SE% = 54%. From pharmacokinetic analysis, the fitted K^{trans} = 0.073/min, and k_{ep} = 0.90/min.
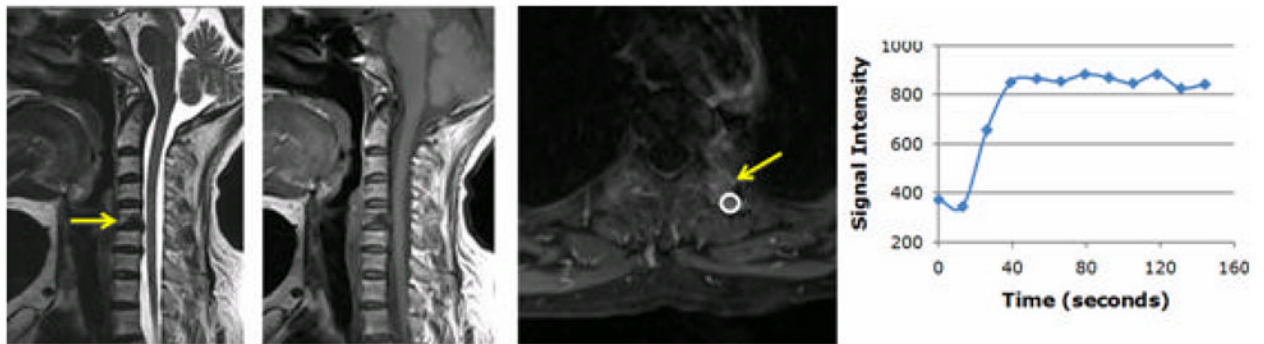
Figure 4.
A 58-year-old female patient with confirmed pathological diagnosis of metastatic cancer originating from the breast. A. MR T2WI and B. MR T1WI show steolytic destruction in the C5 vertebral body. A soft tissue mass is clearly visible. C. Contrast-enhanced MR T1WI shows a heterogeneously enhanced lesion. D. The DCE kinetics show rapid wash-in that reaches a plateau after 40 seconds. The peak SE% = 128%, steepest wash-in SE% = 84% and wash-out SE% = 6%. From pharmacokinetic analysis, the fitted K^{trans} = 0.062/min and k_{ep} = 0.44/min.
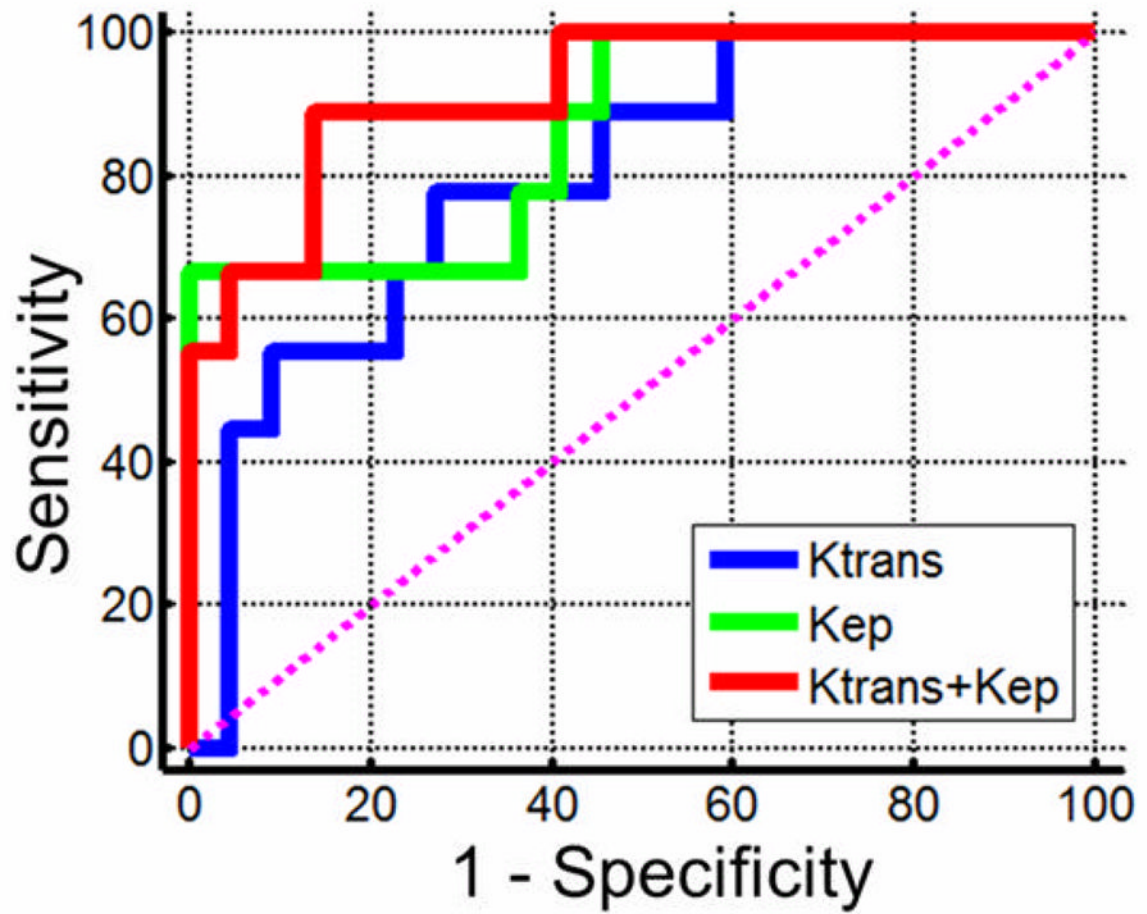
Figure 5.
The ROC curves for differentiating between myeloma and metastatic cancer groups. The area under the curve is 0.798 for K^{trans}, 0.864 for k_{ep}, and an increased 0.919 using combined K^{trans} and k_{ep}.

Table 1

Quantitative parameters analyzed from DCEkinetics of myeloma and metastatic cancer groups

	Peak SE%	Max Wash-in SE %	Ktrans (1/min)	kep (1/min)
Myeloma (N=9)	226 ± 72 %	169 ± 51 %	0.114 ± 0.036	0.88 ± 0.26
Metastasis (N=22)	165 ± 60 %	111 ± 41 %	0.077 ± 0.028	0.49 ± 0.23
P value	0.044	0.010	0.016	0.002

All presented data are group mean ± standard deviation

Table 2

Quantitative parameters analyzed from DCE kinetics of metastatic cancer subgroups with different primary cancer

	Peak SE%	Max Wash-in SE %	Ktrans (1/min)	kep (1/min)	DCE Patterns[†]
Lung (N=7)	159 ± 43 %	104 ± 27 %	0.075 ± 0.020	0.49 ± 0.23	2WO/4PLT/1PSE
Tyroid (N=5) Liver (N=4)	173 ± 45 % 123 ± 19 %	128 ± 44 % 92 ± 20 %	0.083 ± 0.021 0.059 ± 0.011	0.61 ± 0.29 0.44 ± 0.29	4WO/1PSE 2WO/1PLT/1PSE
Breast (N=3)	206 ± 110 %	143 ± 74 %	0.100 ± 0.052	0.53 ± 0.20	2WO/1PLT
Kidney (N=2)	173 ± 122 %	92 ± 51 %	0.080 ± 0.057	0.54 ± 0.22	1WO/1PLT
Prostate (N=1)	199 %	86 %	0.058	0.58	1WO

[†] WO: wash-out pattern; PLT: plateau pattern; PSE: persistent enhancement pattern All presented data are group mean ± standard deviation